Numerical optimization of unsteady natural convection heat transfer from a pair of horizontal cylinders

2016 J. Phys.: Conf. Ser. 745 032080

(http://iopscience.iop.org/1742-6596/745/3/032080)

Numerical optimization of unsteady natural convection heat transfer from a pair of horizontal cylinders

Quentin Pelletier[1*], Tim Persoons, Darina B. Murray

[1] Department of Mechanical and Manufacturing Engineering, Parsons Building, Trinity College, Dublin 2, Ireland

* Corresponding author. Email: pelletiq@tcd.ie

Abstract. This paper presents the results of a numerical study of unsteady natural convection heat transfer from a pair of isothermally heated horizontal cylinders in water. In conjunction with the developed numerical model, a genetic algorithm is designed to search for the optimal spacing between the two cylinders that maximizes their overall heat transfer. When the cylinders are vertically aligned, the heat transfer effectiveness of the upper cylinder is affected by buoyancy-induced fluid flow induced by the lower cylinder. The established and validated CFD model is used to analyse spectral data of local Nusselt number and velocity. The optimization procedure identifies the optimal spacing for Rayleigh numbers ranging from 1e+6 to 1e+7.

1. Introduction

Convective heat transfer from pipes and tubular arrays occurs in many technical applications including heat exchangers, boilers, air cooling systems, etc. Although the time-averaged characteristics of external forced convection from arrays of cylinders are well understood, the understanding of natural convection heat transfer is less complete, especially for confined geometries with strong interactions between the developing thermal plumes and the thermal boundary layer of nearby cylinders. Most studies have focused on the overall heat transfer from a single cylinder [1] or an array of cylinders [2], but not many studies have described the effect of thermal plume oscillations on the transient, local Nusselt number and flow velocity.

Some publications have discussed the swaying motion caused by the thermal plume rising from a single cylinder [3,4] and have characterised its behaviour as a function of Rayleigh number. Numerical studies provide a good body of data for single horizontal heated wires, which can be considered as line heat sources [5-8]. However, only a few studies have investigated the phenomenon for several cylinders.

Studies of the heat transfer from a pair of cylinders has been conducted by Eckert and Soehngen [9] who initially reported enhancement of the heat transfer from the upper cylinder. Previous experimental studies by some of the co-authors [10,11] and Grafsronningen and Jensen [12, 13] confirm either positive or negative enhancement of the upper cylinder's heat transfer, depending on the spacing between the two cylinders. Stafford and Egan [14] report an optimum spacing of $S = 4D$ in the laminar flow regime, for $10^4 \leq Ra \leq 10^5$. The oscillation of the thermal plume has been investigated by Fiscaletti et al. [14] and Kuehner et al. [15, 16] for a single cylinder. Numerical studies report oscillations in the case of a pair of cylinders [17,18]. Many of the numerical investigations that have

been carried out are limited to the two-dimensional approximation. Nevertheless, Desrayaud et al. [8] suggest that time-dependent features possibly emerging in the third dimension are governed by the dynamics on the transverse plane. Hence, results from a two-dimensional analysis can still be of interest, as confirmed by Bastiaans et al. [19].

Persoons et al. [20] describe an experimental study of the coupling between fluid flow and natural convection heat transfer for a pair of vertically aligned cylinders. The transient behaviour of the thermal plume has been characterised for a range of Rayleigh number between 1.7×10^6 and 5.5×10^6 which corresponds to the studied range of Eckert and Soehngen [9]. This previous study by some of the co-authors [20] confirmed a range of cylinder spacing and Rayleigh number where heat transfer from the upper cylinder is enhanced by the plume interaction. However it could only provide hypotheses and partial explanations for the observed phenomena based on the limited amount of experimental data available. Pelletier et al. also report an enhancement of the upper cylinder heat transfer and numerically investigate the correlation between the unsteady velocity field and local Nusselt number [21].

The relation between the enhancement of the overall heat transfer from the pair of cylinders compared to the addition of two single cylinders, and the spacing between the two cylinders, suggest that the search of an optimal distance that could maximize the heat transfer is possible. One of the first evolutionary algorithms was developed by Srinivas & Deb [22] and improved by Deb et al. with the creation of the Non-dominated Sorting Genetic Algorithm II (NSGA-II) [23]. An hybrid variant of the NSGA-II is implemented in Ansys; the Multi-Objective Genetic Algorithm (MOGA).

Based on the previous work from Pelletier et al. [21], in which a numerical model using unsteady Reynolds averaged Navier Stokes computational fluid dynamics is established, validated against previous experimental data [20], and used to reveal the nature of the thermal plume oscillations and their influence on the heat transfer effectiveness, the present paper aims at determining the optimal spacing between the two cylinders using the developed numerical model in conjunction with the MOGA algorithm.

2. Numerical methodology

A numerical model has been developed using ANSYS Fluent 14.0 that aims to provide an estimation of the enhancement or diminishment of the natural convection heat transfer from a pair of horizontal cylinders. The geometrical configuration shown in Fig. 1 is a replica of the test facility used in the experiment conducted by Persoons et al. [20]. This allows the validation of the numerical results by comparison with the experimental results for the ranges of Rayleigh numbers and cylinder spacing that were available from previous work [20]. The experimental approach and results are extensively described by Persoons et al. [20].

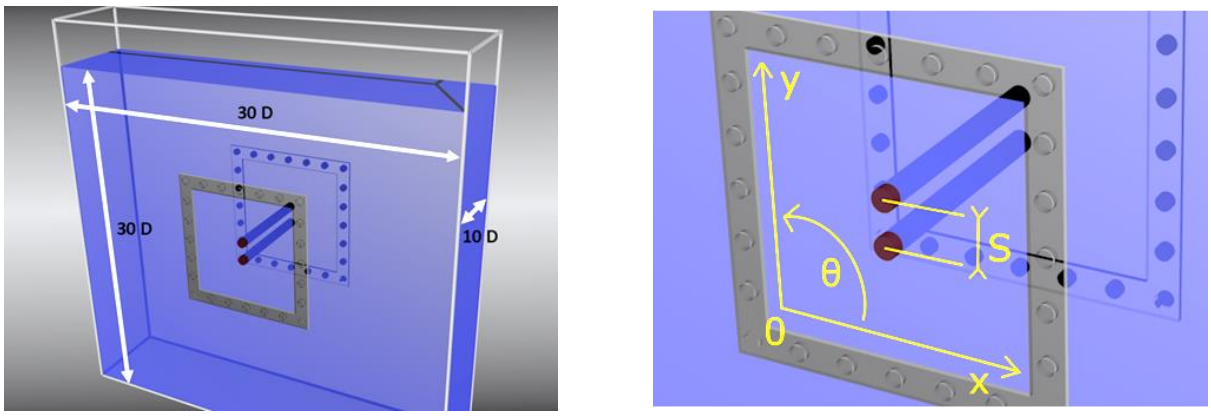

(a) (b)

Figure 1. (a) Diagram of the natural convection geometrical configuration, and (b) close-up view of the cylinder pair.

Both a (steady) Reynolds-Averaged Navier-Stokes (RANS) and Unsteady RANS (URANS) approach are used on a two-dimensional numerical domain. The two-dimensional (2D) approach was used in order to save computational time. The analysis is based on a second order finite volume spatial discretization method for the momentum equation, the PISO velocity-pressure coupling technique (derived from the SIMPLE algorithm [24, 25]) and second order implicit time discretization for the URANS case. The eddy viscosity is obtained using the Shear Stress Transport (SST) $k-\omega$ model with a low-Reynolds model approach to avoid the use of wall functions [24-27]. Since a low-Reynolds model is used, a 2D mesh with 8,600 grid cells is designed to ensure the size of the first cells at the cylinder wall does not exceed $y^+ = 1$. The inner part of the mesh around the cylinders is discretized using quadrilateral cells while the outer part of the numerical domain is discretized with triangular cells as shown in Fig. 2. The skewness and aspect ratio of the cells (triangles as well as quadrilaterals) are minimized (with an average skewness of 0.03 and an average aspect ratio of 1.29) in order to avoid any non-orthogonality related issues.

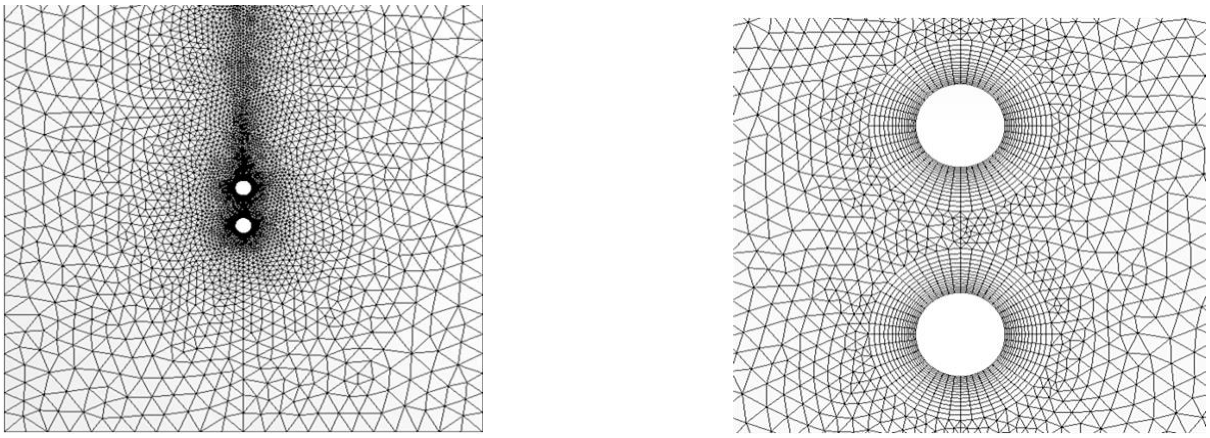

(a) (b)

Figure 2. (a) Overview of the two-dimensional mesh, and (b) close-up view of the pair of cylinders showing the transition from structured mesh around the cylinders to unstructured mesh in the surrounding region.

The fluid density is described by the Boussinesq approximation (Eq. (1)). This is a first order approximation obtained by linearizing the state equation. It is valid for small changes in density, that is to say for $\beta\Delta T \ll 1$. Given the temperature differences involved in this simulation, the Boussinesq approximation can be used in the computation of the buoyancy force term ρg in the momentum equation [24]. Equation (1) expresses a change in temperature as a proportional change in density, and thus enables the simulation of thermally induced gravity driven buoyant motion.

$$\rho(T) = \rho_\infty[1 - \beta(\mathrm{T} - \mathrm{T}_\infty)] \tag{1}$$

where ρ_∞ is the bulk fluid density, T_∞ is the bulk fluid temperature and the thermal expansion coefficient $\beta = -\frac{1}{\rho_\infty}\left(\frac{\partial\rho}{\partial T}\right)_p$. The thermal boundary conditions on the bottom and side walls of the tank are defined as convective boundary conditions, representing the small amount of heat loss through the walls of the tank in the experimental test facility [20]. An overall heat transfer coefficient U is computed as

$$\frac{1}{U} = \frac{1}{h_{water}} + \frac{t_{wall}}{k_{wall}} + \frac{1}{h_{air}} \tag{2}$$

where t_{wall} and k_{wall} are the thickness and thermal conductivity of the tank walls, respectively. h_{water} and h_{air} are the estimated average heat transfer coefficients on the inside (water) and outside (air) of the tank, estimated using established empirical correlations [28]. The top side of the numerical domain is defined as free slip surface to represent the free water surface in the experimental test facility [20].

The mesh size and the time step refinement have been studied for a single cylinder, to ensure that the solution is independent of both mesh size and time step, as explained by Pelletier et al. [21].. For the URANS simulations, a time-step of $\Delta t = 50$ms has been used. A grid size of $\Delta r = 0.5$mm was taken for both steady and URANS simulations. The validation of the model is extensively described by Pelletier et al. [21].

3. Time-averaged, overall results

Results from the RANS simulations can be found in [21]. Table 1 summarizes the numerical results obtain for the heat transfer enhancement in the case of a pair of cylinders;

Table 1. Mean time-average Nusselt number Nu_m of a single cylinder and the upper of a pair of vertically aligned cylinders with the values in brackets representing the relative deviation to a single cylinder, $\delta Nu \times 100\%$. Experimental results from [20].

Case	$Ra = 1.7 \times 10^6$		$Ra = 3.4 \times 10^6$		$Ra = 5.3 \times 10^6$	
	Numerical	Experimental	Numerical	Experimental	Numerical	Experimental
Single cylinder	$Nu_m = 18.3$	$Nu_m = 16.9$	$Nu_m = 21.6$	$Nu_m = 20.7$	$Nu_m = 23.6$	$Nu_m = 23.8$
Upper cylinder ($S = 4D$)	$Nu_m = 19.2$ (+5.0%)	$Nu_m = 18.0$ (+6.1%)	$Nu_m = 23.3$ (+7.7%)	$Nu_m = 22.8$ (+9.2%)	$Nu_m = 24.5$ +4.1%)	$Nu_m = 24.3$ (+2.0%)
Upper cylinder ($S = 3.5D$)					$Nu_m = 26.2$ (+11.0%)	
Upper cylinder ($S = 3D$)	$Nu_m = 19.5$ (+6.5%)	$Nu_m = 18.2$ (+7.2%)	$Nu_m = 23.1$ (+6.8%)	$Nu_m = 22.4$ (+7.6%)	$Nu_m = 26.1$ (+10.8%)	$Nu_m = 26.5$ (+10.2%)
Upper cylinder ($S = 2.5D$)					$Nu_m = 25.6$ (+8.6%)	
Upper cylinder ($S = 2D$)	$Nu_m = 18.1$ (−0.9%)	$Nu_m = 16.1$ (−5.1%)	$Nu_m = 22.3$ (+3.1%)	$Nu_m = 22.3$ (+7.2%)	$Nu_m = 24.7$ (+4.9%)	$Nu_m = 24.5$ (+3.1%)
Upper cylinder ($S = 1.5D$)					$Nu_m = 23.7$ (+0.7%)	

4. Unsteady results

4.1. Spectral analysis of local Nusselt number and flow velocity

Unsteady (URANS) simulations have been performed for each case in Table 1 to further investigate the origin of these oscillations, and their relationship to heat transfer enhancement. The following results corresponds to the configuration $Ra = 3.35 \times 10^6$ and $S = 3D$. As discussed in Section 2, a time step of $\Delta t = 50$ ms has been used. The simulations ran for 80,000 iterations or a simulated time of 4,000 s.

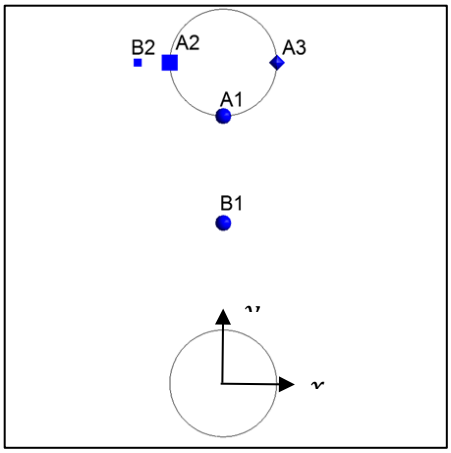

Figure 3. Monitored points where solution data is extracted for FFT spectra and cross spectral density analysis (see Figs. 13-16).

Figure 4 shows quasi-periodic oscillations, where the data in Fig. 4a are obtained from the numerical results and in Fig. 4b from experimental measurements at the same conditions [20]. The strong temporal fluctuations of the local Nusselt number shown in Fig. 4 correspond to lateral swaying oscillations of the thermal plume rising from the lower cylinder.

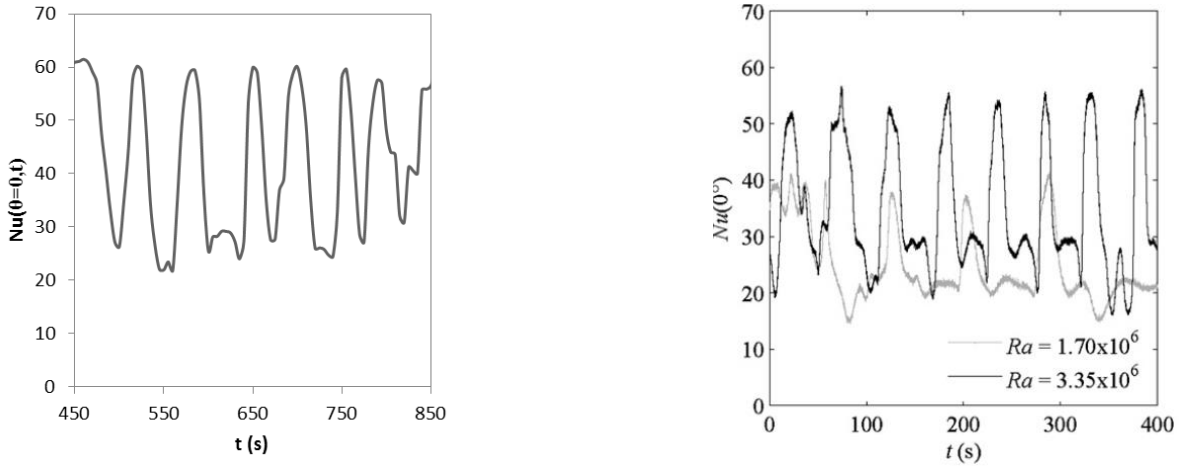

(a) (b)

Figure 4. Time-resolved local Nusselt number at $\theta = 0°$ (point A1 in Fig. 3) for $Ra = 3.35 \times 10^6$, $S = 3D$. (a) Numerical and (b) experimental results [20].

Depending on the time-varying position and shape of the plume, the buoyant flow occasionally impinges directly onto the bottom of the upper cylinder causing a sharp rise in instantaneous local Nusselt number, or it is deflected along either side of the cylinder, causing a reduction in local Nu. The fluid temperature and flow velocity magnitude and direction near the bottom of the upper cylinder (point A1) also vary strongly.

For this same dataset ($Ra = 3.35 \times 10^6$ and $S = 3D$), a frequency analysis of the local Nusselt number at points A1 and A2, and velocity at points B1 and B2 has been performed.

Figure 5 shows the magnitude and phase angle of the cross spectral density between the Nusselt number at point A1 and the velocity components at point B1($C_{A_{1,B_1}}$) (and between the Nusselt number at point A2 and the velocity components at point B2 ($C_{A_{2,B_2}}$).

Three main peak frequencies and their harmonics are be observed on Fig. 5; $f_1 \cong 0.02\ Hz$ and one of its harmonics are marked by a triangle in Fig. 5a. $f_2 \cong 0.01\ Hz$ and some of its harmonics marked by triangles in Fig. 5b and finally $f_3 \cong 0.066\ Hz$ and one of its harmonics marked by circles in Fig. 5b. Frequencies f_1 and f_2 have been identified as frequencies corresponding to the swaying of the thermal plume rising from the bottom cylinder and impinging the top cylinder.

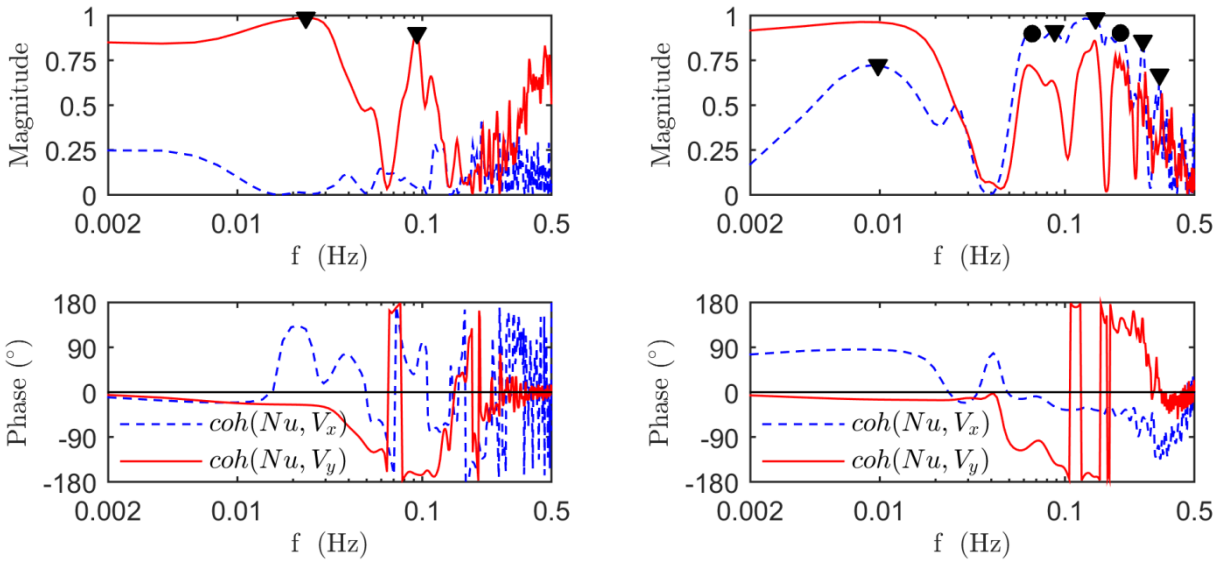

(a) (b)

Figure 5. Magnitude and phase angle of the cross spectral density (a) between local Nusselt number at A1 and velocity components at B1, (b) between local Nusselt number at A2 and velocity components at B2 ($Ra = 3.35 \times 10^6, S = 3D$). Markers indicate two sets of harmonics.

Figure 5a shows that the cross spectral density phase angle near the peak frequency f_1 is slightly negative ($\phi_1 \cong -25°$), which indicates that the Nusselt number at A1 lags the vertical velocity at B1 by $(\phi_1/360)/f_1 \cong 3.6$ s. Considering the distance between locations A1 and B1 (see Fig. 3), one can assume that this lag is mainly due to the time it takes for the rising fluid inside the thermal plume to be advected from point B1 to the stagnation zone near point A1.

Interestingly, Fig. 5b shows a different peak frequency f_3 which is not related to the swaying of the thermal plume and which presents a lag between Nu and V_x of about 0.5 s. This indicates that another periodic pattern is present in the variations of the Nusselt number at point A2 and the horizontal velocity at point B2

The relationship between flow velocity and Nusselt number on the side of the cylinder can lead to a better understanding of how the buoyant plume dynamics affect the heat transfer characteristics of the upper cylinder. An interpretation of these two periodic phenomena (one characterised by f_2 and the other one by f_3) is given in the following sections.

4.2. Discussion: Effect of vortices in the oscillating plume on the local heat transfer coefficient

The higher frequency oscillations represented by f_3 can be explained by the effect of vortices on local instantaneous heat transfer enhancement and can be illustrated by taking a closer look at the time evolution of the local Nusselt number at point A2 and the adjacent transverse (horizontal) velocity V_x

at point B2. As explained in the previous section, the coherence spectrum revealed a strong dependency between these two signals at a peak frequency of $f_3 = 0.06641\ Hz$ between the Nusselt number and the V_x velocity fluctuations which cannot be explained merely by bulk advection.

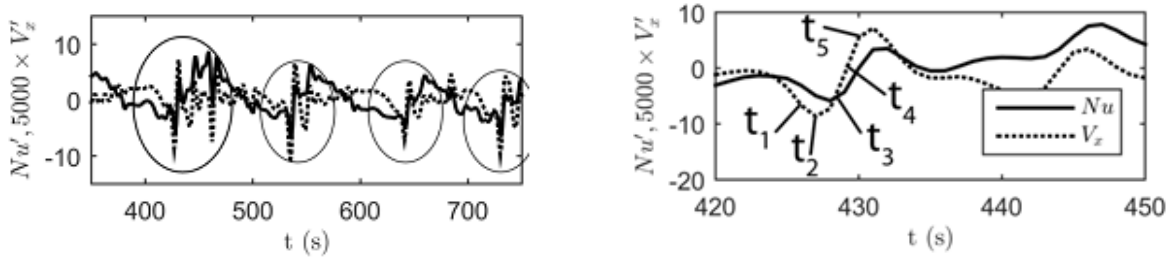

(a) (b)

Figure 6. Fluctuations of the Nusselt number at point A2 and the transverse velocity (arbitrarily scaled) at point B2 ($Ra = 3.35 \times 10^6$, $S = 3D$). Five indicated events in (b) correspond to the flow fields shown in [21], Fig. 21.

Figure 6 shows both signals (with subtracted mean and arbitrarily scaled) for (a) a time duration of 400s, and (b) a close-up view of 30s corresponding to the leftmost encircled interval on Fig. 6a. The two signals are quite similar which confirms the high coherence between them (see Fig. 5b). The four encircled events in Figure 6a exhibit a repeating pattern with a period corresponding to $f_2 \cong 0.0097$ Hz; this corresponds to the plume swaying. However, upon closer inspection each encircled event also contains higher frequency oscillations. Figure 6b shows these oscillations corresponding to the frequency $f_3 = 0.06641\ Hz$ identified in the cross spectral density in Fig. 5. This 'high' frequency oscillation is characterised by a period of approximately $1/f_3 \cong 15\ s$. In terms of Strouhal number, $Sr_3 = f_3 D/V_{ref} \cong 0.58$. A broadly comparable peak frequency was also found experimentally by Persoons et al. [20] ($Sr = 0.46 \pm 0.02$) and Grafsronningen and Jensen [12] ($1/f \cong 7$ s, $S/D = 2$, $Ra = 5.2 \times 10^7$ corresponding to a Strouhal number $Sr = 0.73$).

Persoons et al. present PIV data [20] that show the development and travel of vortices along the top cylinder's edges. These transits correlate with the signals presented in Fig. 6 as discussed by Pelletier et al. [21]. The URANS simulation enabled us to identify how the variations in transverse velocity at point B2 correlate with the variations of Nusselt number at point A2. However, the time-averaged enhancement of the local Nusselt number at point A2 is small ($\delta_{Nu_m(-90°)} = 2.5\ \%$) compared to the enhancement at point A1 ($\delta_{Nu_m(0°)} = 53.6\ \%$) [21]

5. Numerical optimisation of time-averaged overall Nusselt number as a function of spacing S/D

As presented in the previous section, an increase of the overall time-averaged Nusselt number of the top cylinder has been observed. This enhancement appears to be correlated to unsteady phenomena; two main periodic patterns are observed and have been related to local instantaneous enhancement of the heat transfer from the top cylinder.

An optimisation process, based on the NSGA-II genetic algorithm, has been carried out in order to determine the optimal spacing between the two cylinders that maximizes the overall time-averaged heat transfer of the top cylinder. It utilizes the URANS model described in the previous section to run each simulation for 20,000 iterations.

A first optimization is conducted with an initial set of 50 configurations with a Rayleigh number $Ra = 5.33 \times 10^6$ and a spacing varying from $S = 2.8D$ to $S = 4.5D$ in an attempt to find the local optimum for this particular range of spacing, corresponding to the previous work [20,21]. The results of this simulation, presented in Fig. 7, show a convergence of the optimal ratio, when the spacing is constrained in the range $2.8D \leq S \leq 4.5D$, toward a value $S/D_{optimal} \cong 3.65$. This result is in good agreement with the previous investigations [20,21].

The second optimization has been performed over a wider range of spacing ($2 \leq S/D \leq 10$) in an attempt to search for the global optimal spacing that maximizes the overall time-averaged heat transfer. As shown in Fig. 8, the results indicate a convergence of the optimal ratio toward $S/D_{optimal} \cong 7.5$. For this spacing, the top cylinder Nusselt number reaches $\overline{Nu_m} = 30.5$ (as shown in Fig. 8), which corresponds to an enhancement of 20% compared to a single cylinder. Further investigations are currently being conducted to assess the validity of this converged optimum.

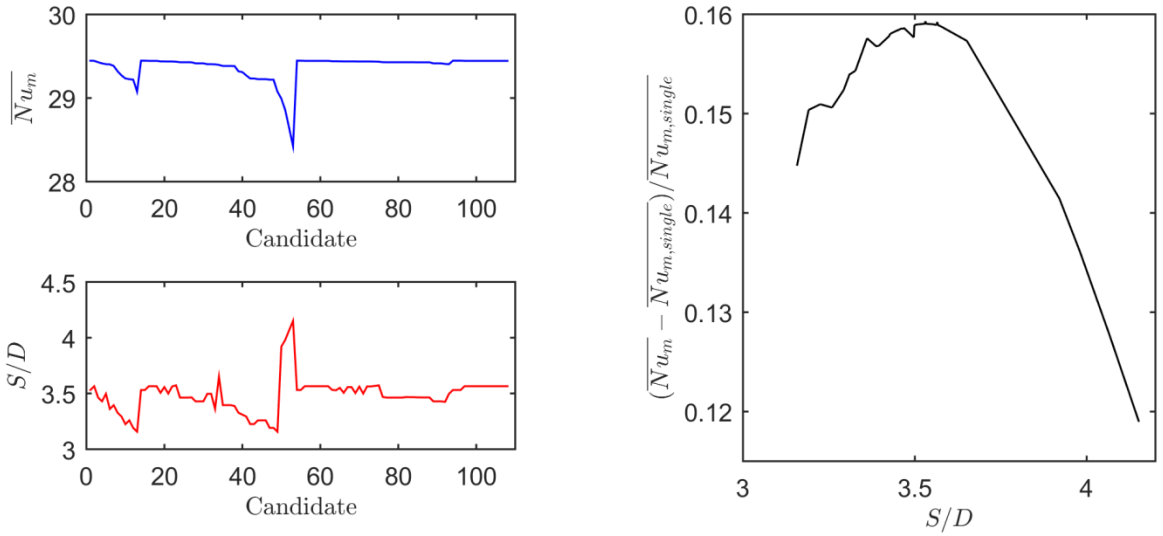

(a) (b)

Figure 7. Local optimum for $2.8 \leq S/D \leq 4$. (a) convergence of the optimal ratio S/D through successive simulations, (b) best suited ratios and corresponding deviation from a single cylinder $\delta Nu_m = \frac{\overline{Nu_m} - \overline{Nu_{m,single}}}{\overline{Nu_{m,single}}}$.

.

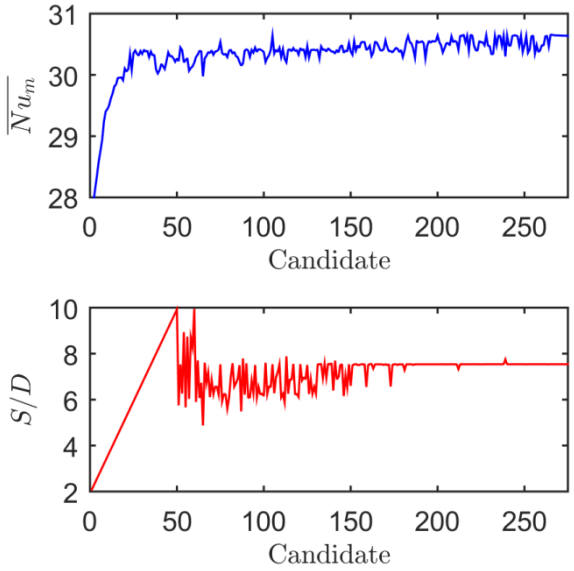

Figure 8. Global optimum ($2 \leq S/D \leq 10$), convergence of the optimal ratio S/D through successive simulations.

6. Conclusion

This paper has presented a numerical study of the transient fluid dynamics and heat transfer in natural convection from a pair of vertically aligned horizontal isothermally heated cylinders, with a centre-to-centre separation distance S ranging from 2 to 4 diameters.

While a previous paper recently published by the authors has focused on the experimental validation of the numerical model [21], the current work has used that validated model and applied numerical optimisation routines using a genetic algorithm to determine the optimal spacing between the cylinders which maximises the time-averaged overall Nusselt number on the upper cylinder.

The optimal spacing was found to be $S/D_{optimal} \cong 6.9$, at which an enhancement in averaged Nusselt number of close to 19% was observed with respect to the isolated cylinder case ate the same Rayleigh number.

7. Acknowledgements

Quentin Pelletier is a PhD research student supported by the Engineering, Energy and Environment (E3) Institute at Trinity College Dublin.

References

[1] Morgan V T 1975 *Adv. Heat Transfer* **11** 199–264
[2] Marsters G F 1972 *Int. J. Heat Mass Transfer* **15** 921-33
[3] Pera L and Gebhart B 1972 *Int. J. Heat Mass Transfer* **15** 177-80
[4] Kitamura K, Kami-iwa F and Misumi T 1999 *Int. J. Heat Mass Transfer* **42** 4093-106
[5] Pera L, Gebhart B and Schorr A W 1970 *Int. J. Heat Mass Transfer* **13** 161-71
[6] Gebhart B and Schorr A W 1970 *Int. J. Heat Mass Transfer* **13** 557-71
[7] Noto K 1989 *J. Thermophys*. **3** 428-34
[8] Desrayaud G and Lauriat G 1993 *J. Fluid Mech*. **252** 617–46.
[9] Eckert E R G and Soehngen E E 1948 *AF Technical report*
[10] O'Gorman I M, Murray D B, Byrne G and Persoons T 2009 *ASME International Mechanical Engineering Congress*
[11] Reymond O, Murray D B and O'Donovan T S 2008 *Exp. Therm. Fluid Sci*. **32** 1702–09
[12] Grafsrønningen S and Jensen A 2012 *Int. J. Heat Mass Transfer* **55** 5552-64
[13] Grafsrønningen S and Jensen A 2013 *Int. J. Heat Mass Transfer* **57** 519-27
[14] Fiscaletti D, Angeli D, Tarozzi L and Barozzi G S 2013 *Int. J. Heat Mass Transfer* **58** 619-31
[15] Kuehner J P, Hamed A M and Mitchell J D 2015 *Int. J. Heat Mass Transfer* **82** 78-97
[16] Kuehner J P, Pflug J R, Tessier F A, Hamed A M and Moiso Marin F J 2012 *Int. J. Heat Mass Transfer* **55** 4711-23
[17] Sebastian G and Shine S R 2015 *Int. J. Heat Mass Transfer* **82** 325-34
[18] Park Y G, Ha M Y, Choi C and Park J 2014 *Int. J. Heat Mass Transfer* **77** 501-18
[19] Bastiaans R J M, Rindt C C M, Nieuwstadt F T M, van Steenhoven A A 2000 *Int. J. Heat Mass Transfer* **43**, 2375–2393
[20] Persoons T, O'Gorman I M, Donoghue D B, Byrne G and Murray D B 2011 *Int. J. Heat Mass Transfer* **54** 5163-72
[21] Pelletier Q, Murray D B and Persoons T 2016 *Int. J. Heat Mass Transfer* **95** 693-708
[22] Srinivas N and Deb K 1995 *IEEE Transactions on evolutionary computation* **2** 221-48
[23] Deb K, Agrawal S, Pratap A and Meyarivan T 2002 *IEEE Transactions on evolutionary computation* **6**
[24] Ansys 2014 *Fluent Documentation*
[25] Issa R I 1986 *J. Comput. Phys.* **62** 40-65
[26] Menter F R and Esch T 2001 *COBEM 16th Brazilian Congress of Mechanical Engineering*.
[27] Menter F R 1994 *AIAA Journal* **32** 1598-1605
[28] Bejan A and Kraus A D 2003 *John Willey & Sons*